Deploying multispectral remote sensing for multi-temporal analysis of archaeological crop stress at Ravenshall, Fife

Revised: 6 June 2018 | Accepted: 18 June 2018

DOI: 10.1002/arp.1721

RESEARCH ARTICLE

WILEY

Deploying multispectral remote sensing for multi-temporal analysis of archaeological crop stress at Ravenshall, Fife, Scotland

Charles Moriarty[1] | Dave C. Cowley[2] | Tom Wade[1] | Caroline J. Nichol[1]

[1] School of GeoSciences, Crew Building, University of Edinburgh, Edinburgh, UK

[2] Historic Environment Scotland, John Sinclair House, Edinburgh, UK

Correspondence
Charles Moriarty, School of GeoSciences, Crew Building, University of Edinburgh, Alexander Crum Brown Road, Edinburgh, EH8 9XP, UK.
Email: charlesdmoriarty@gmail.com

Abstract

Diminishing returns of archaeological crop marks in lowland areas from traditional observer-directed visible spectrum aerial survey with standard photographic cameras highlights a need to explore alternative approaches to maintain the effectiveness of survey programmes. Developments in low-cost multispectral remote sensing have in part been driven by the growth of precision agriculture and, whilst contributing to the intensification of land use, these technologies may offer new spectral and temporal capacities for detecting, recording and monitoring historic landscapes. However, there are significant challenges to the deployment of such approaches, not least the costs of data acquisition and uncertainty about the best conditions for data collection. This study assesses the effectiveness of the Parrot Sequoia, a relatively low-cost multispectral sensor recently developed for agricultural applications, for the detection of crop marks to inform archaeological survey. A series of observations were taken with the sensor mounted on an unmanned aerial vehicle (UAV) at Ravenshall, Fife, Scotland, between April and July 2017. The resulting reflectance maps are compared to red, green and blue (RGB) photographs taken with a Nikon D800E digital camera during seven light aircraft surveys, with the aim of testing the sensors' comparative ability to record crop mark developments over time. The contrast in reflectance between vegetation samples growing over buried archaeological remains and the surrounding field was assessed through separability in regional histogram values across different image band combinations. Separable values indicative of crop marks were found in both the multispectral and RGB results from June 2017 onwards. Several vegetation index (VI) maps, particularly the Simple Ratio (SR) and Normalised Difference Vegetation Index (NDVI), were found to be effective for distinguishing crop marks in the multispectral results. The Sequoia is a cost-effective sensor offering improved spectral resolution over the RGB photographs, showing potential for subtle crop mark detection across compact study areas.

KEYWORDS

aerial photography, agriculture, archaeological survey, multispectral remote sensing, unmanned aerial vehicles (UAVs), vegetation indices

1 | INTRODUCTION

In many parts of the landscape archaeological knowledge is heavily dependent on the observation of vegetation proxies that reveal otherwise buried remains (Jones & Evans, 1975; Wilson, 2000). This is especially true in lowland areas, where such crop marking across arable fields is a primary source of archaeological information. In Scotland, for example, the phenomenon of crop marking has been recognised since at least the 1920s, with annual programmes of airborne reconnaissance conducted by a variety of agencies since 1945

and continuing under the auspices of Historic Environment Scotland (HES) to the present (Cowley, 2016). Cumulatively, this work has placed over 9000 monuments on record, in many areas providing the majority of the archaeological evidence for past settlement and land use (Figure 1) (Cowley, Hale, Hunter, & Macleod, 2009; Maxwell & St Joseph, 1983). Traditionally, crop marks have been observed and recorded in the visible wavelengths of the electromagnetic spectrum, typically recording reflected red, green and blue (RGB) light equivalent to wavelengths visible to the human eye (in broad bands centred approximately around 670, 550 and 450 nm respectively) (Bennett, Welham, Hill, & Ford, 2013; Verhoeven & Doneus, 2011). While this approach has revolutionised knowledge of lowland areas, in many areas a pattern of diminishing returns from survey can be seen (Cowley, 2016), indicating that the traditional survey approach is losing value in providing new information. This is evident in the fluctuating numbers of newly discovered monuments in East Lothian, southeast Scotland, from 1945 to 2015 (Figure 2). The low level of discoveries from 1945 to 1974 is the product of reconnaissance by J. K. St Joseph of Cambridge University as part of a national programme of aerial survey in the United Kingdom. From 1975/1976 more regular reconnaissance was undertaken from Edinburgh, which ensured greater intensity of survey. While levels of returns from survey were maintained through the 1990s, the overall pattern has been for fewer previously unknown sites to be discovered. This pattern applies equally to the Ravenshall area and other parts of lowland Scotland, and is not an artefact of differential survey intensity as reconnaissance has been conducted in all but the wettest years. The ongoing effectiveness of traditional survey is being affected by changes in land use, with farming practice developing to offset the crop stress that the airborne archaeologist relies on to see buried remains, while climate change also appears to be playing a role in reducing variable response to buried features in growing crops, especially during wetter summers (Figure 3). The historical perspective on the impact that varying climatic conditions have on returns from traditional aerial reconnaissance, provided by comparing Figures 2 and 3, highlights this pattern of diminishing returns. This also poses a challenge to survey projects that undertake reconnaissance over limited periods of a few years to assess their rates of recovery against long-term data in order to contextualise their results. These issues present a fundamental challenge to archaeological prospection, and interest in multispectral and hyperspectral sensors, capable of detecting electromagnetic radiation in a number of broad or narrow wavelength bands both including and outside the visible spectrum, have led to studies on how these can be effectively utilised to detect contrasts in vegetation reflectance beyond the spectral and temporal observing windows of RGB photography (Aqdus, Hanson, & Drummond, 2012; Beck, 2011; Berni, Zarco-Tejada, Suarez, & Fereres, 2009;Doneus, Verhoeven, Atzberger, Wess, & Ruš, 2014; Morgan, Gergel, & Coops, 2010; Verhoeven & Doneus, 2011).

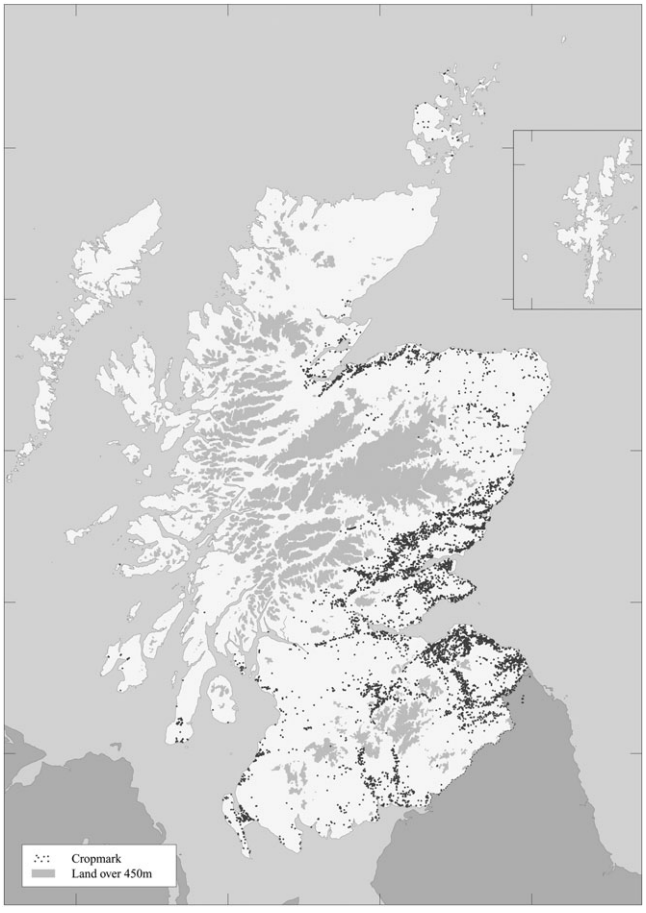

FIGURE 1 The distribution of archaeological sites recorded as crop marks across Scotland. The majority have been identified during observer-directed aerial survey and documented on traditional photographs. In areas of well drained soils set to arable in relatively drier parts of the country this approach has provided the majority of archaeological knowledge on the disposition of past settlement and land use remains. GV004748 © Historic Environment Scotland

Hyperspectral sensors offer a wider range of observing bands than multispectral sensors, yet at present have a high associated cost. Compounded by a limited understanding of the conditions under which spectral responses in vegetation may be most effectively recorded, this makes it difficult to leverage such data in an affordable way. For these reasons, recent developments in low-cost multispectral remote sensing technologies, driven by the agricultural and ecological sectors, are of considerable interest as a more cost-efficient means of broadening our understanding of the archaeological potential of these technologies and the optimal timing for their deployment. Understanding the benefits and limitations of these sensors compared to traditional photography is vital to ensure the historical record can be efficiently surveyed, documented and managed in the face of change (De Guio, 2015; Verhoeven & Sevara, 2016). Whilst the application of these technologies to precision agriculture may accelerate the threat to site conservation, they may also be harnessed to improve our understanding and detection capacity of arable landscapes (De Guio, 2015).

The study reported on here aimed to assess the potential of a low-cost multispectral sensor for detecting vegetation change across archaeological features over time in comparison to standard aerial photography. Utilising a four-band Parrot Sequoia sensor designed for precision agriculture, mounted on an unmanned aerial vehicle (UAV), three multispectral surveys were undertaken between April and July 2017 in Fife, Scotland, over a field with a known history of crop marks. This is the first time this sensor, released in 2016, is

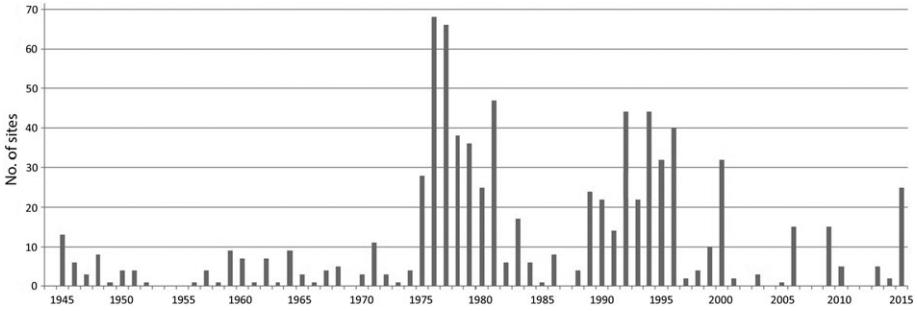

FIGURE 2 The fluctuating numbers of newly discovered monuments in East Lothian, Southeast Scotland, from 1945 to 2015 illustrate the returns from relatively low intensity of survey in the period 1945–1974. While the increased returns from the mid-1970s are a product of greater survey intensity, the fluctuations from year to year are primarily a product of varying weather patterns (see Figure 3). The peak in discoveries in 2015 is mainly due to large numbers of amorphous remains and field boundaries being documented, sites that would not have been considered meriting record in the past. © Historic Environment Scotland

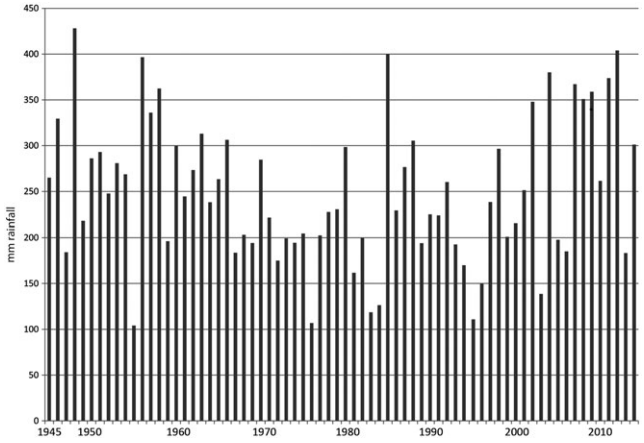

FIGURE 3 The average summer rainfall in eastern Scotland in the period from 1945 to 2015. The dramatic year to year variation has a profound impact on the potential for crop mark formation, and dry years generally correlate with high incidences of crop marks (see Figure 2). When seen over a 70-year period the disproportionate impact that rare very dry years have had on site discovery is clear when compared with the rates of newly discovered sites shown in Figure 2 (Met Office, 2018)

known to have been used for crop mark archaeology. Contrasts in reflectance between regions of archaeological interest and their surroundings, across different band combinations, are compared to regional contrast in RGB photographs taken with a Nikon D800E camera during seven light aircraft surveys by HES over the course of the season. The differences observed have been examined alongside regional soil moisture deficit measurements to investigate the climatic conditions associated with detectable changes in the crops. This study testing the Sequoia forms part of a larger project exploring how multispectral and hyperspectral imaging can be effectively deployed as part of a national archaeological survey strategy.

1.1 | Background

A well-established relationship has been identified between buried archaeological features and the surface vegetation that grows above them (Jones & Evans, 1975; Verhoeven & Doneus, 2011; Wilson, 2000). These effects are usually observed in cultivated fields, where plough-levelled remains can have a longstanding, seasonal effect on agricultural crops, though in extreme conditions grass can also be affected. The influence of buried archaeological remains may be evident in the height of the local crop canopy, and/or the reflectance signature of the vegetation, producing areas of local contrast known as crop marks. The extent to which crops are affected by this process varies depending on the crop type, health and climate, and the formation of crop marks may vary dramatically from year to year (Cowley, 2011). Crop marks will appear and change dynamically across a phenological cycle and are considered to be most evident during a crops boot stage, as a local soil moisture deficit develops (Agapiou, Hadjimitsis, & Alexakis, 2012; Agapiou, Hadjimitsis, Sarris, Georgopoulos, & Alexakis, 2013; Aqdus et al., 2012). The archaeological interpretation of crop marks is almost entirely driven by consideration of the geometry and context of crop colour variances and occasionally height.

Archaeological research has focussed on how developments in remote sensing platforms and sensors can be utilised for detection of crop marks, as well as how improvements in software and analytical techniques can augment processing and interpretation (Atzberger, Wess, Doneus, & Verhoeven, 2014; Beck, 2011; Bennett, Cowley, & De Laet, 2014; Campana, 2017; Lasaponara & Masini, 2012). Multispectral or hyperspectral remote sensing provides an avenue to detect changes in crop health through observed reflectance, whilst height data from airborne laser scanning (ALS) or image-based modelling (IBM) can be used to study structural changes in crop canopies or wider changes in the landscape. This can be particularly useful in conjunction with imaging to observe both spectral and topographical change (Kincey et al., 2014; Neubauer et al., 2014; Opitz & Cowley, 2013; Rowlands & Sarris, 2007; Verhoeven & Vermeulen, 2016).

Early studies utilising multispectral sensors for archaeology found that by creating false colour composite (FCC) images utilising different wavelength bands, particularly around the red-edge (~700 nm) and near infrared (NIR) (~700–1100 nm) wavelengths, crop marks could be visualised more clearly than through a true colour image, occasionally revealing previously unidentified features (Cavalli, Colosi, Palombo, Pignatti, & Poscolieri, 2007; Donoghue & Shennan, 1988; Powlesland et al., 2006). More recent studies have looked at how wider ranges of spectral information captured by both airborne and spaceborne multispectral sensors may be most effectively, and subjectively, exploited for archaeological prospection particularly in

comparison to aerial photography (Agapiou et al., 2012; Bennett et al., 2013; Doneus et al., 2014; Traviglia, 2006; Verhoeven & Sevara, 2016). Different vegetation indices (VIs), mathematical combinations of observed wavelength bands, have been widely studied in the search for improved visual enhancements in processed images (Agapiou et al., 2012; Bennett et al., 2013; Bennett, Welham, Hill, & Ford, 2012; Cerra, Agapiou, Cavalli, & Sarris, 2018; Challis, Kincey, & Howard, 2009; De Guio, 2015; Traviglia, 2006; Verhoeven & Doneus, 2011). Over 150 VIs have been utilised across different studies (Bennett et al., 2012) although their comparative effectiveness for crop mark detection has been found to vary depending on observing conditions (Agapiou et al., 2012; Aqdus et al., 2012; Aqdus, Drummond, & Hanson, 2008; Bennett et al., 2012; Cerra et al., 2018; Challis et al., 2009). Whilst there has been criticism that VIs are often applied haphazardly, without appropriate consideration of the vegetation properties they have been formulated to highlight, they are still commonly used for their simplicity and effectiveness in highlighting contrasts in vegetation health (Agapiou, Lysandrou, Lasaponara, Masini, & Hadjimitsis, 2016; De Guio, 2015). Indeed, recent work (Cerra et al., 2018) has evaluated a range of VIs to provide objective means of comparing information return through the application of information theory. Alternative approaches have looked at information extraction techniques beyond the use of simple band algebra, such as Principal Component Analysis (PCA) or Tasselled Cap Transformations (TCTs) to transform spectral data into new information components that minimise redundancy, or the work by Doneus et al. (2014) on visualising the red-edge inflection point and distribution of a crop's reflectance curve (Agapiou et al., 2016; Agapiou, Alexakis, Sarris, & Hadjimitsis, 2013; Aqdus et al., 2012; Bennett et al., 2013; Cavalli et al., 2007; Challis et al., 2009; Doneus et al., 2014; Lasaponara & Masini, 2007; Traviglia, 2006). There is an ongoing challenge to developing universally effective crop mark enhancement techniques as the most appropriate methodology will vary depending on the sensor spectral resolution, the type of landscape and stage of the growing season (Agapiou et al., 2016; Verhoeven & Sevara, 2016), and relatively few multi-temporal studies have investigated how analytical techniques perform over an extended observing period (Agapiou et al., 2012; Agapiou, Hadjimitsis, et al., 2013; Bennett et al., 2013). However, extensive studies by Agapiou on a test site in Cyprus have explored how the performance of VIs changes over a phenological cycle, although these results have yet to be tested outside of the Mediterranean, or in comparison to RGB photography (Agapiou et al., 2012). Ecological studies have explored the use of lightweight multispectral sensors on UAVs for exploring crop stress at finer spatial resolutions than higher altitude aerial or satellite surveys (Berni et al., 2009), but these sensors have yet to be extensively investigated in archaeological applications.

In this context, the present study is timely in exploring the archaeological potential of an affordable sensor, and studying the changing character of crop marks and spectral characteristics of the crop over parts of the growing season.

2 | STUDY AREA AND DATA ACQUISITION

Ravenshall is an arable field of 5.5 ha located at Raecruick Farm, Fife, Scotland (56° 16′ 31″ N 3° 12′ 25″ W, in the WGS 84 coordinate system) (Figure 4), in which winter wheat (*Triticum aestivum*) was growing during the observing season (planted 29 September 2016). The site lies in an area known as the Howe of Fife with extensive archaeological remains recorded as crop marks over many decades of aerial reconnaissance (Cowley & Gilmour, 2005; Maxwell, 1983; see also

FIGURE 4 The location of the test site at Ravenshall in east-central Scotland, with an oblique aerial photograph of the field taken on 17 July 2017 (Basemap source: Esri/World Imagery). Inset © Historic Environment Scotland

https://canmore.org.uk). The field for the test site reported on here was chosen for having a series of well-documented crop marks, observed during aerial survey and recorded on oblique aerial photographs spanning 40 years. The aspiration for the study was to collect regular multispectral surveys over the growing season from April to June, perhaps as often as two-weekly, supplemented by RGB photography and less regular hyperspectral imaging. In the event, combinations of variable weather conditions and technical difficulties, meant that a total of three multispectral surveys were conducted, on 17 April, 5 May and 12 July 2017, supplemented by RGB photography on seven occasions (see later). The multispectral surveys utilised a Parrot Sequoia sensor (Parrot SA, Paris, France) mounted on a Tarot 680Pro hexacopter, a custom-built UAV. The Sequoia is a four-band sensor designed for precision agriculture, consisting of one RGB and four multispectral cameras, recording data in the green, red, red-edge and NIR wavelength bands (Table 1) (Parrot Drones, 2017). The red-edge is an area of steep reflectance change between red to NIR wavelengths, with a shifting transition point dependent on vegetation type and health, which is commonly identified around 700 nm – this is regarded as a key point for detecting vegetation variation for archaeological purposes (Verhoeven & Doneus, 2011). Centred around 735 nm, the Sequoia's 'red-edge' band lies just outside of the wavelength range that is generally regarded as susceptible to red-edge shifts (690–730 nm) (Carter, Estep, & Muttiah, 2002), providing interesting additional data on the efficiency of this band for detecting stress. The Sequoia was chosen for the multispectral component of this study due to its relatively low cost, its light weight and its design for detecting changes in vegetation health.

TABLE 1 Specifications for the parrot Sequoia (Parrot Drones, 2017)

Main unit	
Dimensions	59 mm × 41 mm × 28 mm
Mass	72 g
RGB camera	
Resolution	16MP
Image size	4608 × 3456 pixels
Shutter release	Electronic rolling shutter
Focal length	4.88 mm
Multispectral camera	
Pixel count	1.2MP
Image size	1280 × 960 pixels
Shutter release	Electronic global shutter
Focal length	3.98 mm
Wavelengths	Green 550 nm (40 nm width)
	Red 660 nm (40 nm width)
	Red-edge 735 nm (10 nm width)
	Near infrared 790 nm (40 nm width)
Additional features	Inertial measurement unit (IMU), magnetometer
Sunshine sensor	
Dimensions	47 mm × 39.6 mm × 18.5 mm
Weight	35 g
Spectral sensors	Green, red, red-edge, near infrared
Additional features	Global positioning system (GPS), IMU, magnetometer

Surveys were flown using the open-source Mission Planner autopilot software (ArduPilot Dev Team, 2016) at an altitude of 60 m, velocity of 4 m/s and calculated image overlap of 70%. This allowed the field extent to be covered in two flights of approximately 10–15 minutes duration each, with an average ground sampling distance of 1.55 cm/pixel for the RGB camera and 6.00 cm/pixel for the multispectral cameras. Illumination conditions during flights were recorded by the Sequoia 'Sunshine' sensor, and spectrally calibrated MicaSense reflectance panels were photographed before and after each flight to support radiometric calibration during image processing. Ongoing regional soil moisture deficits were recorded from the Met Office Rainfall and Evapo-transpiration Calculation System (MORECS). These deficits are calculated for grass environments in a 40 km grid and provided a relative measure of regional moisture levels across the observing period. The test site was also recorded on seven occasions from 3 May to 18 July 2017, using a handheld Nikon D800E digital camera (Nikon Corporation, Japan) to capture RGB images (Table 2). These photographs were taken out of an open window from a Cessna 172 fixed-wing light aircraft flying at approximately 2000 ft (610 m).

2.1 | Processing

Digital surface maps (DSMs) and orthomosaics of the field were created using Structure-from-Motion (SfM) based software, referencing 26 fixed ground control points (GCPs) that were installed around the perimeter of the field and measured to 0.5–3.5 cm accuracy using a Trimble differential global navigation satellite system (GNSS). Pix4Dmapper Pro (Version 3.1.23.0) was used for orthomosaic generation and radiometric calibration of the Sequoia TIFF data and the RGB photographs were processed in TIFF format through Agisoft PhotoScan (Version 1.3.4).

Two classification regions were defined across the field from rectified oblique aerial photographs from the last 40 years and the derived interpretative archaeological mapping. Firstly, 'object' areas were chosen across regions where geometric shapes corresponded

TABLE 2 Specifications for the Nikon D800E (Nikon corporation, 2017)

Main unit	
Dimensions	146 mm × 123 mm × 81.5 mm
Mass	1000 g
Camera	
Pixel count	36MP
Image size	7360 × 4912 pixels (maximum format)
Shutter release	Mechanical focal-plane shutter
50 mm Lens	
Dimensions	72 mm (diameter) × 52.5 mm
Weight	185 g
Focal length	50 mm
28–70 mm Lens	
Dimensions	88.5 mm (diameter) × 121.5 mm
Weight	935 g
Focal length	28–70 mm (set to 50 mm)

to the interpreted archaeological mapping, and were evident in multiple current and historic image layers. Secondly, 'field' areas where no mapped archaeology was present (Figure 5). The field samples were chosen to be adjacent to object samples where possible, to allow contrast to be studied between potential archaeology and its immediate context.

Image products were created from the multispectral and RGB data with the aim of testing visualisation methods from other crop mark studies and comparing the results from the two sensors. For each multispectral survey date, the red, green, red-edge and NIR orthomosaics created by Pix4D were converted into four-band stacked images to allow for FCC visualisation of different band channels in ENVI (Version 5.2). These were then transformed in ArcGIS into principal component images, linear combinations of the initial data into four new bands that maximise variance across the pixel values (Lillesand & Kiefer, 2000). The new components were also used for FCC visualisations, found by other studies to potentially improve contrast in areas of crop stress over the original bands. FCC images, principal component images and 16 VI maps were generated from each set of multispectral data, with the aim of testing and extending the work of other studies (Agapiou et al., 2012; Aqdus et al., 2012; Bennett et al., 2012, 2013; Challis et al., 2009). A full list of VIs generated can be found in Table 3. RGB photographs were converted to greyscale in QGIS Desktop (Version 2.14.3) to compress the three bands of information into a single band for analysis. This allowed the single band results to be assessed using the same measure as the multispectral index maps, discussed later. The greyscale conversion utilised the luma Y'_{709} weighting coefficients (Kanan & Cottrell, 2012):

$$\text{Grey} = 0.2126\times\text{Red} + 0.7152\times\text{Green} + 0.0722\times\text{Blue}$$

The ability to discriminate between object and field regions across the image products was examined by studying the separability in pixel values between the defined object and field sample areas. The multiband Sequoia images were assessed using the Jeffries–Matusita (J–M) Distance, a known statistical parameter calculated directly within ENVI (Kumar et al., 2016; Lillesand & Kiefer, 2000). For single-band images, including the VI products and RGB greyscale conversions, the separability between histograms for the two samples was assessed using the M-Statistic (Kaufman & Remer, 1994). This measure takes into account the mean (μ) and standard deviation (σ) of both samples, with values of $M > 1$ indicating strongly separable histograms:

$$M = \frac{|\mu_1 - \mu_2|}{\sigma_1 + \sigma_2}$$

The J–M Distance and M-Statistic have been used to assess spectral separability (e.g. Kumar et al., 2016) of different types of crop classified from multispectral satellite image data. A flow diagram of the steps from data acquisition to analysis is provided in Figure 6.

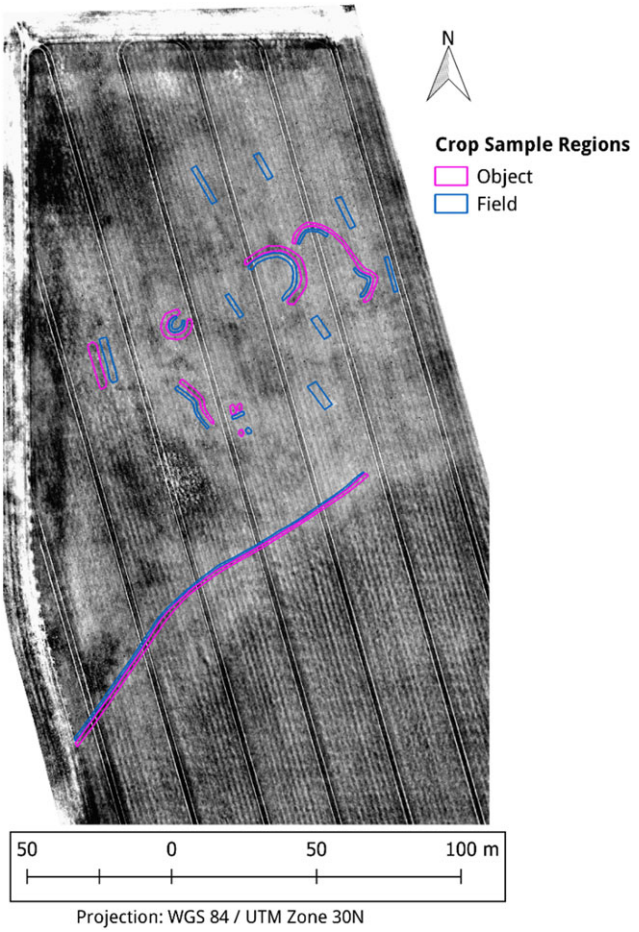

FIGURE 5 Locations of the two crop regions defined for analysis, overlaid on the 12 July 2017 Simple Ratio (Near Infrared/Red) index map [Colour figure can be viewed at wileyonlinelibrary.com]

3 | RESULTS

Referencing the perimeter GCPs, the orthomosaics generated for each individual survey had root mean square (RMS) errors in the *x*–*y* plane ranging between 1.1 and 8.0 cm in both Pix4D and PhotoScan models. Elevation had a higher error range of between 27 and 57 cm, apart from the 12 July 2017 orthomosaic which had *z*-error of up to 2.46 m. This is believed to be due to issues with detecting the elevated fence line used for mounting several of the GCPs in the vertical imagery, as well as the reduced accuracy of the internal global positioning system (GPS) of the Sequoia. It should be noted that the centre of the field has lower positional accuracy due to its increased distance from the referenced perimeter (and a restriction on placing GCPs in the area of growing crop). A maximum of 25.7 cm elevation difference was found between the two closest surveys (17 and 18 July), which was considered to be too high an error to study changes in crop height alongside the spectral results (Verhoeven & Vermeulen, 2016). However, a raised area was noted in the north half of the field across all DSMs, notably in the area where most of the mapped archaeology has been identified, corresponding to a slight rise visible in the surface topography.

The spectral separability of the object and field sample regions was calculated for each multispectral survey across the 16 VI products. Values were also calculated for the RGB imagery, to show the spectral separability across the uncalibrated red, green and blue camera bands. This provides an assessment of VI performance by indicating how well the two regions may be distinguished after applying each index, as well as an indication of the dynamics of change over time (Table 4). Whilst little separability was observed in the April and May

TABLE 3 List of Vegetation Indices (VIs) used to create index maps from the multispectral data, including formulae and index details

Index	Abbreviation	Formula	Application
Normalised Difference Vegetation Index	NDVI	$\frac{\rho_{NIR}-\rho_{RED}}{\rho_{NIR}+\rho_{RED}}$	Measuring green vegetation through normalised ratio ranging from −1 to 1.
Green Normalised Difference Vegetation Index	GNDVI	$\frac{\rho_{NIR}-\rho_{GREEN}}{\rho_{NIR}+\rho_{GREEN}}$	Modification to NDVI, more sensitive to chlorophyll concentration.
Red-Edge Normalised Difference Vegetation Index	RENDVI	$\frac{\rho_{750}-\rho_{705}}{\rho_{750}+\rho_{705}}$	Modification to NDVI, utilising red-edge information to probe for changes in vegetation health.
Normalised Difference Red-Edge/Red	NDRER	$\frac{\rho_{RED-EDGE}-\rho_{RED}}{\rho_{RED-EDGE}+\rho_{RED}}$	Modification to NDVI, utilising red-edge information in place of near infrared (NIR) reflectance.
Optimised Soil Adjusted Vegetation Index	OSAVI	$\frac{1.5(\rho_{NIR}-\rho_{RED})}{\rho_{NIR}+\rho_{RED}+0.16}$	Variation to NDVI to reduce the effect of soil reflectance in areas with partial vegetation cover using standardised values.
Simple Ratio	SR	$\frac{\rho_{NIR}}{\rho_{RED}}$	Ratio of NIR scattering to chlorophyll absorption, used for simple vegetation distinction.
Modified Simple Ratio	MSR	$\frac{\left(\frac{\rho_{NIR}}{\rho_{RED}}\right)-1}{\left(\sqrt{\frac{\rho_{NIR}}{\rho_{RED}}}\right)+1}$	A combination of renormalised NDVI and SR to improve sensitivity to vegetation characteristics.
Green Ratio Vegetation Index	GRVI	$\frac{\rho_{NIR}}{\rho_{GREEN}}$	Modification to simple ratio, sensitive to rates of photosynthesis.
Red Green Ratio Index	RGRI	$\frac{\rho_{RED}}{\rho_{GREEN}}$	Used to indicate leaf production and stress. Traditionally calculated as the ratio of the mean of all red bands to green bands, in this case the single red and green bands have been used.
Nonlinear Vegetation Index	NLI	$\frac{\rho_{NIR}^2-\rho_{RED}}{\rho_{NIR}^2+\rho_{RED}}$	Modification to NDVI to emphasise linear relationships with vegetation parameters.
Modified Chlorophyll Absorption Ratio Index	MCARI	$[(\rho_{700}-\rho_{670})-0.2(\rho_{700}-\rho_{550})]\frac{\rho_{700}}{\rho_{670}}$	An indication of levels of chlorophyll, adjusted to minimise soil background effects.
Transformed Chlorophyll Absorption Reflectance Index	TCARI	$3\left[(\rho_{700}-\rho_{670})-0.2(\rho_{700}-\rho_{550})\left(\frac{\rho_{700}}{\rho_{670}}\right)\right]$	Similar to MCARI, used to indicate chlorophyll levels. Sequoia red-edge, red and green reflectance has been substituted for the traditional narrowband wavelengths.
Modified Triangular Vegetation Index	MTVI	$1.2[1.2(\rho_{800}-\rho_{550})-2.5(\rho_{670}-\rho_{550})]$	Used to estimate changes in leaf area and canopy structure.
Plant Senescence Reflectance Index	PSRI	$\frac{\rho_{680}-\rho_{500}}{\rho_{750}}$	Used to study the ratio between bulk carotenoids and chlorophyll, to study stress and senescence. Sequoia red, green and NIR reflectance has been substituted for the traditional narrowband wavelengths.
Anthocyanin Reflectance Index 2	ARI1	$\frac{1}{\rho_{550}}-\frac{1}{\rho_{700}}$	Used to measure stressed vegetation through sensitivity to anthocyanin content.
Anthocyanin Reflectance Index 2	ARI2	$\rho_{800}\left[\frac{1}{\rho_{550}}-\frac{1}{\rho_{700}}\right]$	Modification to ARI1, with increased sensitivity to anthocyanin content.

Note: Agapiou et al., 2012, 2016; Agapiou, Hadjimitsis, et al., 2013; Bennett et al., 2012; Birth & McVey, 1968; Challis et al., 2009; Deering, 1978; Jordan, 1969; Pearson & Miller, 1972; Verhoeven & Doneus, 2011. ρ_{GREEN}, ρ_{RED}, $\rho_{RED\text{-}EDGE}$, ρ_{NIR}: reflectance across broad green, red, red-edge and near infrared wavelength bands. $\rho_{wavelength}$: reflectance across narrow bands corresponding to the denoted wavelength. For use in this study, the closest Sequoia reflectance bands have been substituted for the traditional narrow band wavelengths.

multispectral observations ($M < 0.1$), following the 14 June survey a visible distinction across the designated crop mark regions appears in the imagery, corresponding with values of $M > 0.1$. Older aerial photographs of the site, where crop marks show a high degree of visual contrast, were found to have benchmark separability figures of up to 0.69. From this study, 14 June and 17 July were found to have the highest greyscale separability, while the best performing VI maps in the 12 July multispectral survey were found to be the Simple Ratio/Modified Simple Ratio (SR/MSR), Normalised Difference Vegetation Index (NDVI) and Anthocyanin Reflectance Index 2 (ARI2) (Figure 7). The RGB separability observed across each survey date has been plotted against ongoing MORECS data in Figure 8. It is noted that the emergence of crop marks in the 14 June imagery, reflected in high separability values, appears following the period of greatest soil moisture deficit, as might be expected (Jones & Evans, 1975).

To investigate the ability to identify archaeologically-influenced change using the SR, the mean change between each survey date was calculated for the two sample areas, with the object region found to have a higher mean change (2.50) between May and July than the field sample (1.78). An image threshold was applied to highlight all areas with change above this mean, which were found to lie both within and outside areas of archaeological interest (Figure 9). This

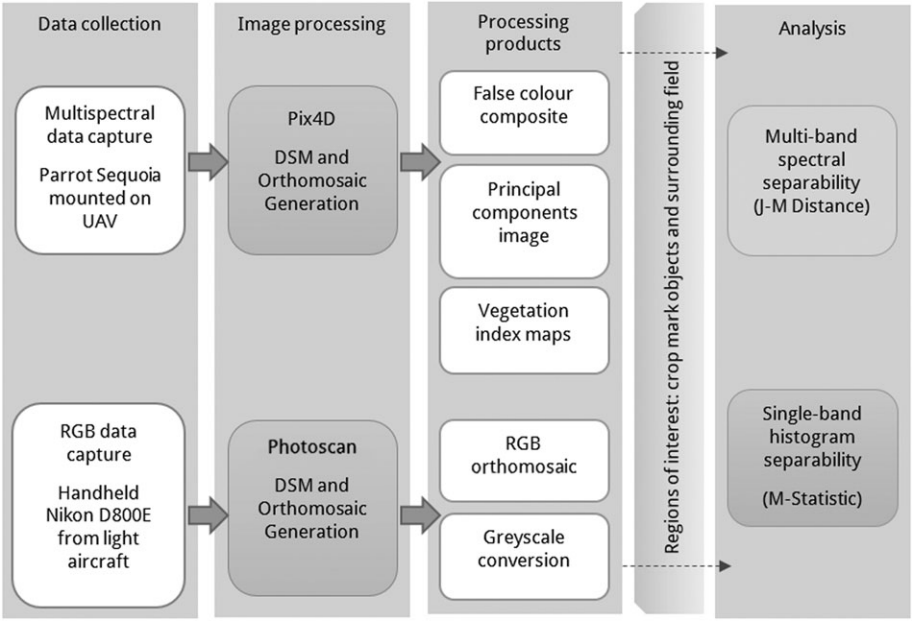

FIGURE 6 Flow diagram detailing the processing stages from data collection to analysis

method offered some advantages to visualisation, yet the poor signal-to-noise ratio for the time interval under consideration makes it challenging to clearly isolate archaeological change from these values.

4 | DISCUSSION

In this study, crop stress influenced by archaeological remains was successfully detected in multispectral imagery from the Parrot Sequoia. In the early stages of crop growth, during the 17 April and 5 May surveys, regions designated as object and field showed little separability across individual bands and band combinations ($M < 0.098$). On 12 July, these regions were observed to have changed at different rates, showing greater histogram separability across several bands. From the VIs tested, variants of the Simple Ratio (SR, MSR, GRVI), NDVI (NDVI, GNDVI) and ARI2 produced the highest degree of separability between the two sampled regions. This supports results from other studies, which have found the SR to be one of the most effective band combinations for highlighting crop marks (Agapiou et al., 2012, 2016; Bennett et al., 2012). When assessed in isolation, the red and green bands were more effective for detecting change across the sample region than the individual red-edge and NIR bands. Ongoing surveys would aid in assessing whether the Sequoia's red-edge band improves in performance as the crop continues to mature, or if this band indeed lies too far beyond the typical red-edge wavelength range to be useful for clearly identifying stress.

Crop marks were also detected in the RGB aerial photographs visually from 14 June onwards, which corresponded to greyscale histogram separabilities of $M > 0.107$. It is important to note that the RGB data was not radiometrically calibrated and shows some illumination variation between surveys, which will affect the M-statistic results calculated. However, this effect is not regarded as significant in the current dataset, with the aerial surveys flown under generally similar conditions. For future studies an additional radiometric calibration step that normalises RGB illumination from ground measurements or areas of known reflectance in the image would improve the accuracy of the M-statistic results (Verhoeven, 2009; Verhoeven & Sevara, 2016). The Sequoia's RGB camera was found to have poor image quality compared to the Nikon D800E, with high noise levels affected by small photosites, as well as significant geometric distortion due to the electronic rolling shutter.

A key advantage to the UAV-mounted Sequoia multispectral camera over the RGB aerial photography is the increased spatial and spectral resolution. This is evident in Figure 10, where finer detail across regions of crop stress appears in the multispectral index map created with the narrow bands of the Sequoia than in the RGB greyscale transformation. This has positive implications for being able to detect smaller and subtler objects within the multispectral imagery.

Limitations to the Sequoia sensor include the overall practicality for deployment. Whilst RGB surveys were undertaken as part of wider area aerial sorties, across a broader range of dates, the Sequoia flight time and range was limited by the battery capacity and UAV line-of-sight regulations, and choice of survey date was constricted by weather. The cost of the Sequoia sensor is relatively low (~£3000), providing affordable multispectral imaging capability in specific contexts. However, surveys required a half-day for equipment preparation and flight over a comparatively small area, and generated a much larger file set than the RGB imagery. Accurately measured GCPs were essential for generating orthomosaics from the imagery and would need to be located across the landscape in a larger area survey. Thus, while the Sequoia provided a high-resolution, effective method for detecting changes in crop health across a compact site, it is less practical for larger areas. Tests of the equipment on a fixed wing UAV with greater endurance would assist in determining the potential range achievable for ongoing surveillance, though it would not achieve levels of coverage of the modified and calibrated digital camera setup recommended by Verhoeven and Sevara (2016) (~£170 000).

TABLE 4 M-statistic indicating separability of digital number histograms for object and field sample regions of interest across different image dates and products

Date	Greyscl.	Green	Red	Red-edge	NIR	PCA (B2)	ARI1	ARI2	GNDVI	GRVI	MCARI	MSR	MTVI	NDVI	NLI	OSAVI	PSRI	RENDVI	RGRI	SR	TCARI	NDRER
17 April 2017	0.127	0.098	0.088	0.038	0.052	0.044	0.090	0.084	0.096	0.083	0.059	0.067	0.068	0.082	0.073	0.077	0.028	0.064	0.053	0.058	0.059	0.081
3 May 2017	0.047																					
5 May 2017	0.092	0.095	0.066	0.037	0.005	0.072	0.095	0.071	0.083	0.073	0.018	0.049	0.033	0.063	0.048	0.052	0.012	0.085	0.025	0.041	0.018	0.054
25 May 2017	0.089																					
14 June 2017	0.224																					
20 June 2017	0.125																					
3 July 2017	0.107																					
12 July 2017	0.096	0.160	**0.311**	0.044	0.038	0.297	0.207	**0.339**	**0.332**	**0.338**	0.154	**0.377**	0.081	**0.358**	0.187	0.177	0.065	0.238	0.210	**0.380**	0.154	0.293
17 July 2017	0.319																					
18 July 2017	0.216																					

Note: Multispectral vegetation indices (VIs) with a separability of $M > 0.3$ are highlighted in bold.

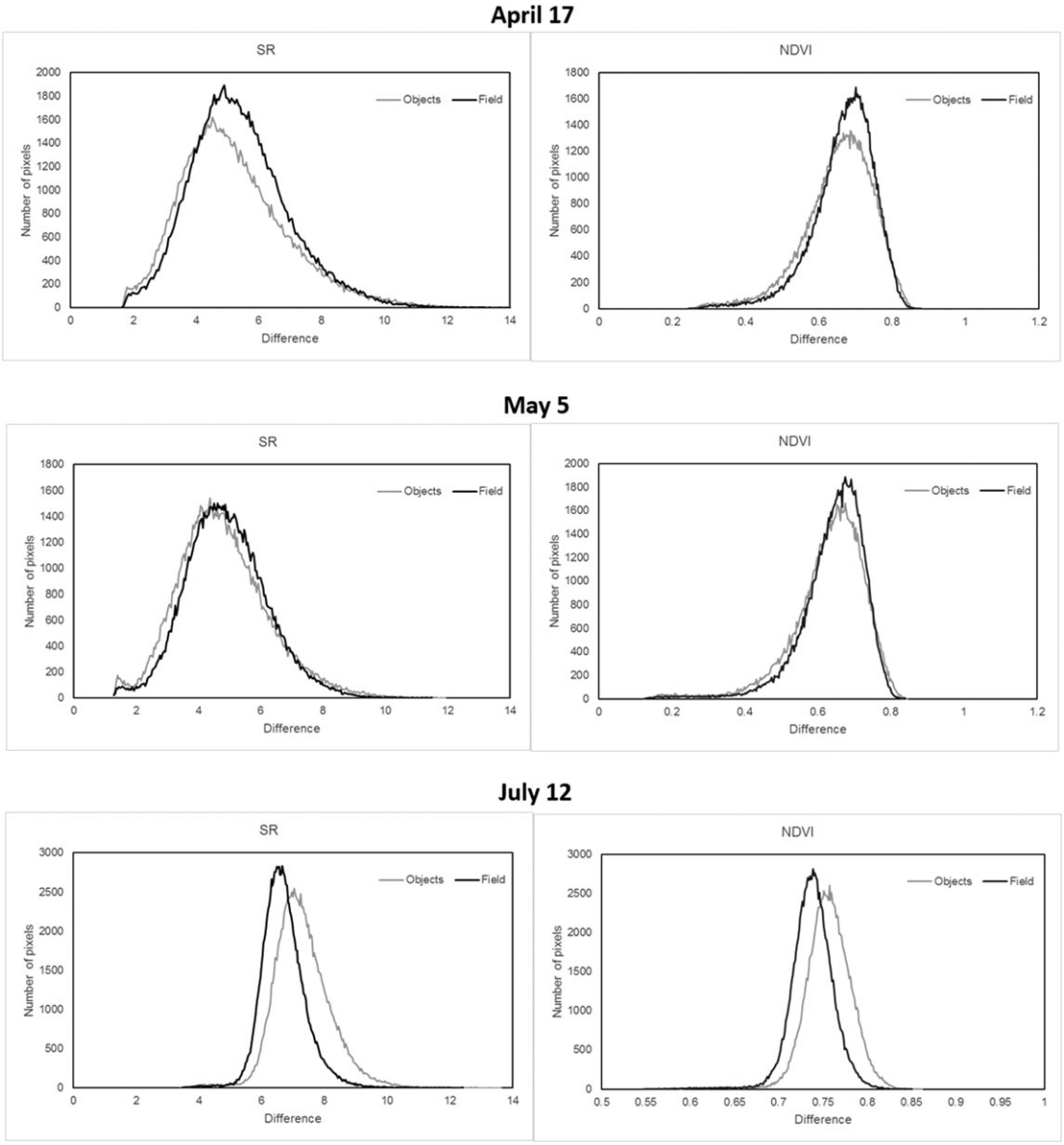

FIGURE 7 Comparison of Simple Ratio (SR) and Normalised Difference Vegetation Index (NDVI) histograms for the object and field sample regions across the three multispectral image dates

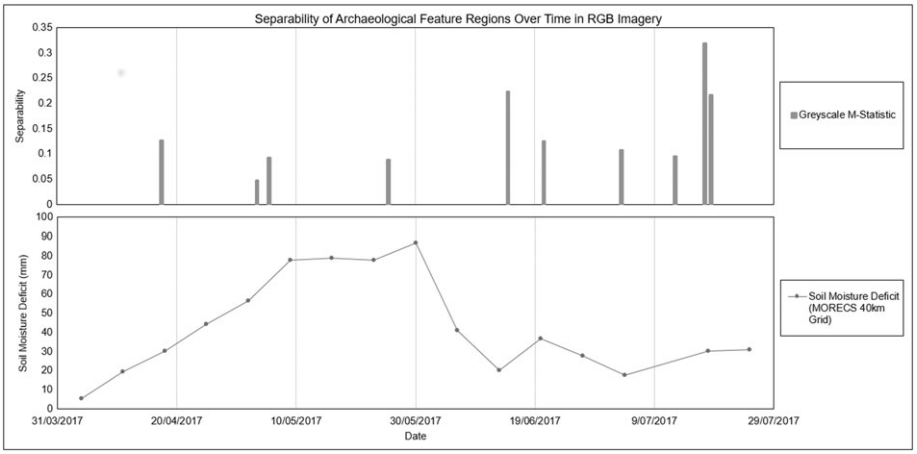

FIGURE 8 Separability of archaeological objects over time, showing histogram separability (M-statistic) calculated for greyscale conversions of the RGB imagery, with ongoing soil moisture deficits within a 40 km regional grid shown below

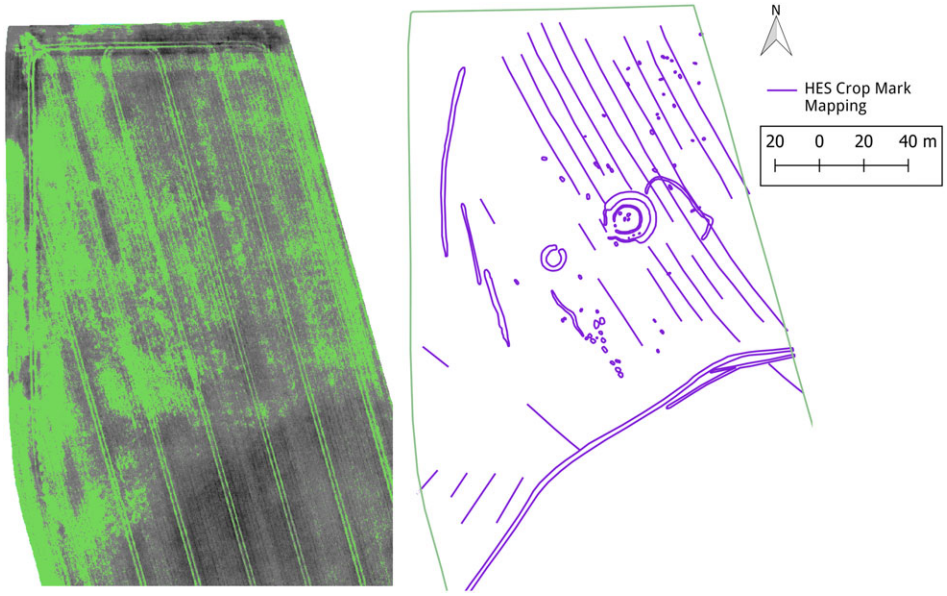

FIGURE 9 Simple Ratio change map between May and July 2017, with areas of greater than 2.5 units change highlighted in green, compared to Historic Environment Scotland (HES) crop mark mapping for reference. © Historic Environment Scotland [Colour figure can be viewed at wileyonlinelibrary.com]

FIGURE 10 Comparison of image detail in multispectral index map (12 July 2017 Simple Ratio, left) to RGB photograph (17 July 2017 greyscale conversion, right). © Historic Environment Scotland

An outstanding question in assessing the sensor is whether a larger number of, or different, archaeological features may be identified in the multispectral imagery over RGB photographs. While Bennett et al. (2012) were able to compare imaging techniques through a count of number of features detected, the crop stress detected in the current dataset was not clearly discriminated into distinctive features other than the sample used in the change comparison. This may be due to the phenological window of crop growth observed, as marks may become more distinct as the crop continues to mature (Agapiou, Hadjimitsis, et al., 2013), or it may be due to 2017 being a relatively poor year for crop mark development, with a dry spring followed by a wetter than average summer (Met Office, 2017). The results provide an insight into the response of the crops to broad-ranging soil moisture deficits measured between April and July, with a notable emergence of crop marks in RGB photographs following the period of greatest soil moisture deficit in May.

To compare the two sensors under study and assess the level of detectable change, it was necessary to define regions of the field considered to be proxies for buried archaeology. This limits the outputs of the study to objects previously identified from the RGB photographs. This is a source of bias introduced through the limitation of the RGB imagery and serves to exclude regions that may be subject to more subtle stress, or which may contain unidentified archaeological remains. This also assumes that all crop areas within the sample

changed at equivalent rates; average separabilities may not be representative of all objects within the region. Due to the variations in crop reflectance observed broadly across the field, the choice of sample sites is likely to have a strong effect on results and may be subject to noise from soil, weeds, underlying geology and errors in the orthomosaic generation. The accuracy of the results will also be affected by radiometric error within the Sequoia sensor itself. The wavelength bands have been assumed to follow the manufacturer-quoted specifications; a valuable additional step would be to conduct a ground spectrometer comparison to confirm the accuracy of the measurements collected by the Sequoia and calibrated by the software (Berni et al., 2009). Improving the vertical accuracy during DSM-creation would open up additional possibilities for exploring crop surface maps in relation to the spectral results, which would be achievable through the placement of GCPs across the field site as well as along the perimeter (Verhoeven & Vermeulen, 2016).

Histogram separability is one measure of distinguishing whether the two samples possess different reflectance properties, yet it should be noted that the values found are all lower than statistically confirmable separability ($M > 1$ or $J–M > 1.7$). Separability values of $M > 0.1$ were found to correlate to changes detectable with the human eye, although this underscores the challenge of avoiding observer bias in crop mark identification. A probabilistic approach, comparing the samples to a randomly generated set of intensities, might aid in confirming the robustness of the results. It is also important to note that both the J–M Distance and M-Statistic provide measures of intensity difference between regions, but are not always directly comparable to differences observed with the human eye, which also considers factors such as object shape and context. More crop marks can be manually distinguished in the 3 July greyscale image ($M = 0.107$) than the 17 April greyscale image ($M = 0.127$), providing an example of how noise in the sample can affect histogram separability values and the caution that should be taken when interpreting the M-statistic results. As the two samples are not statistically separable across the spectrum, it was not possible to reliably classify areas of archaeologically-influenced crop stress through the thresholding method that was attempted. Visualisation techniques such as contrast stretching or false colour mapping can aid the ability to visually distinguish crop marks and exaggerate regional separabilities, yet the information an observer draws from these image products will be highly subjective, again emphasising the difficulty in comparing separability results to visual judgement.

5 | CONCLUSIONS AND FUTURE WORK

A Parrot Sequoia multispectral sensor has been utilised to target the detection of archaeologically-influenced crop stress: the first time this sensor is known to have been tested for this purpose. From surveys taken over April to July 2017 at Ravenshall, Fife, changes in reflectance were successfully detected across regions of archaeological interest compared to a sample of surrounding field points, at equivalent timings to RGB photography. An ideal next step would be to continue surveys beyond the duration of this study to assess the continued performance of the Sequoia across later stages of the phenological cycle. Additional multispectral surveys during the crop mark emergence period in June, which were not performed due to weather limitations, would aid quantification of the timing of crop mark emergence as detected by the two sensors. Expanding the study area to include different crop types, which possess different reflectance properties and phenological cycles, would further assist with a study of relative timing and to examine variations in red-edge responses. A comparison with other sensor types, for example a hyperspectral sensor offering finer spectral resolution, would be beneficial in determining the comparative efficiency of the Sequoia. The Sequoia offers advantages over RGB photography in terms of spectral resolution across a targeted site, with advantages to spatial resolution through the use of a low-altitude drone for observations, although RGB imagery remains a reliable and consistent method for detecting crop marks as proxies for archaeology and may continue to be more practical on a broader landscape scale. Utilising the Sequoia for supporting RGB observations over specific sites of interest could be a cost-effective and beneficial means of assessing the amount of archaeological information that can be recorded (e.g. Cowley et al., 2018).

At present archaeological crop mark identification relies largely on traditional observer-directed manual approaches, which brings with it the issues of confirmation bias and the limitations of an entirely human based visible spectrum approach to image analysis. As semi-automated approaches to analysis are explored, it will be vital to have data that can support discrimination between archaeological regions of crop stress independent of prior sources of bias (Bennett et al., 2014; Cerra et al., 2018; Traviglia, Cowley, & Lambers, 2016). Whilst the change detected in both the multispectral and RGB results from this study was partially defined by visual analysis, the separability found shows promise that as analytical techniques develop (including methods such as edge detection, unsupervised classification and object-based image analysis), change regions may be automatically rather than manually classified. This will certainly be vital to the strategic assessment of large area datasets from satellites or fixed wing aircraft – a development that is necessary to explore means of redressing the diminishing returns from traditional observer-directed visible spectrum aerial survey. Future work in refining methods to detect change, particularly for datasets where spectral differences are subtle, is a key next step in remote sensing for archaeology (Bennett et al., 2014; Traviglia et al., 2016). Whilst the interpretation of crop marks as proxies for archaeological remains may always require some level of human judgement, the ability to recognise these features across different spatial and spectral windows continues to be improved by new sensor technologies.

ACKNOWLEDGEMENTS

This research was conducted as a collaboration between the University of Edinburgh's School of GeoSciences and Historic Environment Scotland. The authors would like to thank Adara López-López and Jakob Assmann for their assistance, Raecruick Farm for their accommodation of the study, and Geert Verhoeven for his invaluable feedback on early results.

ORCID

Dave C. Cowley http://orcid.org/0000-0001-8197-260X

Caroline J. Nichol http://orcid.org/0000-0003-4177-1787

REFERENCES

Agapiou, A., Alexakis, D., Sarris, A., & Hadjimitsis, D. (2013). Orthogonal equations of multi-spectral satellite imagery for the identification of un-excavated archaeological sites. *Remote Sensing*, *5*(12), 6560–6586. https://doi.org/10.3390/rs5126560

Agapiou, A., Hadjimitsis, D., & Alexakis, D. (2012). Evaluation of broadband and narrowband vegetation indices for the identification of archaeological crop marks. *Remote Sensing*, *4*(12), 3892–3919. https://doi.org/10.3390/rs4123892

Agapiou, A., Hadjimitsis, D. G., Sarris, A., Georgopoulos, A., & Alexakis, D. D. (2013). Optimum temporal and spectral window for monitoring crop marks over archaeological remains in the Mediterranean region. *Journal of Archaeological Science*, *40*(3), 1479–1492. https://doi.org/10.1016/j.jas.2012.10.036

Agapiou, A., Lysandrou, V., Lasaponara, R., Masini, N., & Hadjimitsis, D. (2016). Study of the variations of archaeological marks at Neolithic site of Lucera, Italy using high-resolution multispectral datasets. *Remote Sensing*, *8*(9), 723. https://doi.org/10.3390/rs8090723

Aqdus, S. A., Drummond, J., & Hanson, W. S. (2008). Discovering archaeological cropmarks: A hyperspectral approach. *The International Archives of the Photogrammetry, Remote Sensing and Spatial Information Sciences*, *XXXVII*(B5), 361–366.

Aqdus, S. A., Hanson, W. S., & Drummond, J. (2012). The potential of hyperspectral and multi-spectral imagery to enhance archaeological cropmark detection: A comparative study. *Journal of Archaeological Science*, *39*(7), 1915–1924. https://doi.org/10.1016/j.jas.2012.01.034

ArduPilot Dev Team. (2016). Mission Planner Home - Mission Planner documentation. Retrieved July 18, 2018, from http://ardupilot.org/planner/index.html

Atzberger, C., Wess, M., Doneus, M., & Verhoeven, G. (2014). ARCTIS — a MATLAB® toolbox for archaeological imaging spectroscopy. *Remote Sensing*, *6*(9), 8617–8638. https://doi.org/10.3390/rs6098617

Beck, A. (2011). Archaeological applications of multi/hyper-spectral data–challenges and potential. In D. Cowley (Ed.), *Remote sensing for archaeological heritage management: Proceedings of the 11th EAC Heritage Management Symposium, Reykjavík, Iceland, 25–27 March 2010* (pp. 87–97). Brussels, Belgium: Europae Archaeologia Consilium (EAC).

Bennett, R., Cowley, D., & De Laet, V. (2014). The data explosion: Tackling the taboo of automatic feature recognition in airborne survey data. *Antiquity*, *88*(341), 896–905.

Bennett, R., Welham, K., Hill, R. A., & Ford, A. (2012). The application of vegetation indices for the prospection of archaeological features in grass-dominated environments: Application of vegetation indices in grass-dominated environments. *Archaeological Prospection*, *19*(3), 209–218. https://doi.org/10.1002/arp.1429

Bennett, R., Welham, K., Hill, R. A., & Ford, A. (2013). Airborne spectral imagery for archaeological prospection in grassland environments—An evaluation of performance. *Antiquity*, *87*(335), 220–236. https://doi.org/10.1017/S0003598X00048730

Berni, J., Zarco-Tejada, P. J., Suarez, L., & Fereres, E. (2009). Thermal and narrowband multispectral remote sensing for vegetation monitoring from an unmanned aerial vehicle. *IEEE Transactions on Geoscience and Remote Sensing*, *47*(3), 722–738. https://doi.org/10.1109/TGRS.2008.2010457

Birth, G. S., & McVey, G. R. (1968). Measuring the color of growing turf with a reflectance spectrophotometer. *Agronomy Journal*, *60*(6), 640. https://doi.org/10.2134/agronj1968.00021962006000060016x

Campana, S. (2017). Drones in archaeology. State-of-the-art and future perspectives. *Archaeological Prospection*, *24*(4), 275–296. https://doi.org/10.1002/arp.1569

Carter, G. A., Estep, L., & Muttiah, R. S. (2002). General spectral characteristics of leaf reflectance responses to plant stress and their manifestation at the landscape scale. In R. S. Muttiah (Ed.), *From laboratory spectroscopy to remotely sensed spectra of terrestrial ecosystems* (pp. 271–293). Dordrecht, The Netherlands: Kluwer Academic Publishers.

Cavalli, R. M., Colosi, F., Palombo, A., Pignatti, S., & Poscolieri, M. (2007). Remote hyperspectral imagery as a support to archaeological prospection. *Journal of Cultural Heritage*, *8*(3), 272–283. https://doi.org/10.1016/j.culher.2007.03.003

Cerra, D., Agapiou, A., Cavalli, R. M., & Sarris, A. (2018). An objective assessment of hyperspectral indicators for the detection of buried archaeological relics. *Remote Sensing*, *10*(4), 500. https://doi.org/10.3390/rs10040500

Challis, K., Kincey, M., & Howard, A. J. (2009). Airborne remote sensing of valley floor geoarchaeology using Daedalus ATM and CASI. *Archaeological Prospection*, *16*(1), 17–33. https://doi.org/10.1002/arp.340

Cowley, D. (2011). Remote sensing for archaeology and heritage management – site discovery, interpretation and registration. In D. Cowley (Ed.), *Remote sensing for archaeological heritage management: Proceedings of the 11th EAC Heritage Management Symposium, Reykjavík, Iceland, 25–27 March 2010* (pp. 43–55). Brussels, Belgium: Europae Archaeologia Consilium (EAC).

Cowley, D. (2016). Creating the cropmark archaeological record in East Lothian, south-east Scotland. In R. Crellin, C. Fowler, & R. M. Tipping (Eds.), *Prehistory without borders: The prehistoric archaeology of the Tyne-Forth region* (pp. 59–70). Oxford, UK: Oxbow Books.

Cowley, D., Moriarty, C., Geddes, G., Brown, G., Wade, T., & Nichol, C. (2018). UAVs in context: Archaeological airborne recording in a national body of survey and record. *Drones*, *2*(1), 2.

Cowley, D. C., & Gilmour, S. M. (2005). Discovery from the air: A pit-defined cursus monument in Fife. *Scottish Archaeological Journal*, *25*(2), 171–178.

Cowley, D. C., Hale, D. N., Hunter, F., & Macleod, K. H. J. (2009). Survey in the Traprain Law Environs Project area. In C. Haselgrove (Ed.), *The Traprain Law Environs Project – fieldwork and excavations 2000–2004* (pp. 11–21). Edinburgh, UK: Society of Antiquaries of Scotland.

De Guio, A. (2015). Cropping for a better future: Vegetation Indices in Archaeology. In A. Chavarria Arnau, & A. Reynolds (Eds.), *Detecting and understanding historic landscapes* (pp. 109–152). Mantova: SAP Società Archaeologica s.r.l.

Deering, D. W. (1978). Rangeland reflectance characteristics measured by aircraft and spacecraft sensors (PhD thesis). Texas A &M University, College Station, TX (PhD thesis).

Doneus, M., Verhoeven, G., Atzberger, C., Wess, M., & Ruš, M. (2014). New ways to extract archaeological information from hyperspectral pixels. *Journal of Archaeological Science*, *52*, 84–96. https://doi.org/10.1016/j.jas.2014.08.023

Donoghue, D., & Shennan, I. (1988). The application of remote sensing to environmental archaeology. *Geoarchaeology*, *3*(4), 275–285.

Jones, R. J. A., & Evans, R. (1975). Soil and crop marks in the recognition of archaeological sites by air photography. In D. A. Wilson (Ed.), *Aerial reconnaissance for archaeology*. London, UK: Council for British Archaeology.

Jordan, C. F. (1969). Derivation of leaf-area index from quality of light on the forest floor. *Ecology*, *50*(4), 663–666. https://doi.org/10.2307/1936256

Kanan, C., & Cottrell, G. W. (2012). Color-to-grayscale: Does the method matter in image recognition? *PLoS One*, *7*(1), e29740. https://doi.org/10.1371/journal.pone.0029740

Kaufman, Y. J., & Remer, L. A. (1994). Detection of forests using mid-IR reflectance: An application for aerosol studies. *IEEE Transactions on Geoscience and Remote Sensing*, *32*(3), 672–683. https://doi.org/10.1109/36.297984

Kincey, M., Batty, L., Chapman, H., Gearey, B., Ainsworth, S., & Challis, K. (2014). Assessing the changing condition of industrial archaeological remains on Alston moor, UK, using multisensor remote sensing. *Journal of Archaeological Science*, *45*, 36–51. https://doi.org/10.1016/j.jas.2014.02.008

Kumar, P., Prasad, R., Choudhary, A., Mishra, V. N., Gupta, D. K., & Srivastava, P. K. (2016). A statistical significance of differences in classification accuracy of crop types using different classification algorithms. *Geocarto International*, 1–19. https://doi.org/10.1080/10106049.2015.1132483

Lasaponara, R., & Masini, N. (2007). Detection of archaeological crop marks by using satellite QuickBird multispectral imagery. *Journal of Archaeological Science*, *34*(2), 214–221. https://doi.org/10.1016/j.jas.2006.04.014

Lasaponara, R., & Masini, N. (Eds.) (2012). *Satellite remote sensing: A new tool for archaeology*. Dordrecht, The Netherlands: Springer.

Lillesand, T. M., & Kiefer, R. W. (2000). *Remote sensing and image interpretation* (4th ed.). New York: John Wiley & Sons.

Maxwell, G. S. (1983). Recent aerial survey in Scotland. In G. S. Maxwell, & J. K. S. St Joseph (Eds.), *The impact of aerial reconnaissance on archaeology* (pp. 27–40). London, UK: Council for British Archaeology.

Maxwell, G. S., & St Joseph, J. K. S. (Eds.) (1983). *The impact of aerial reconnaissance on archaeology*. London, UK: Council for British Archaeology.

Met Office. (2017). 2017 weather summaries. Retrieved April 15, 2018, from https://www.metoffice.gov.uk/climate/uk/summaries/2017

Met Office. (2018). Met Office Hadley Centre Observation Data. Retrieved April 22, 2018, from https://www.metoffice.gov.uk/hadobs/hadukp/data/download.html

Morgan, J. L., Gergel, S. E., & Coops, N. C. (2010). Aerial photography: A rapidly evolving tool for ecological management. *Bioscience*, *60*(1), 47–59. https://doi.org/10.1525/bio.2010.60.1.9

Neubauer, W., Gugl, C., Scholz, M., Verhoeven, G., Trinks, I., Löcker, K., … Meirvenne, M. V. (2014). The discovery of the school of gladiators at Carnuntum, Austria. *Antiquity*, *88*(339), 173–190. https://doi.org/10.1017/S0003598X00050298

Nikon Corporation. (2017). Nikon Digital SLR Camera D800/D800E Specifications. Retrieved January 28, 2018, from http://imaging.nikon.com/lineup/dslr/d800/spec.htm

Opitz, R. S., & Cowley, D. (2013). *Interpreting archaeological topography: Airborne laser scanning, 3D data and ground observation*. Oxford, UK: Oxbow Books.

Parrot Drones SA. (2017). Parrot Sequoia Technical Specifications. Retrieved January 28, 2018, from https://www.parrot.com/us/Business-solutions/parrot-sequoia#technicals

Pearson, R. L., & Miller, L. D. (1972). Remote mapping of standing crop biomass for estimation of the productivity of the shortgrass prairie, Pawnee National Grasslands, Colorado. In *Proceedings of the Eighth International Symposium on Remote Sensing of Environment, October 2–6, 1972* (pp. 1355–1379).

Powlesland, D., Lyall, J., Hopkinson, G., Donoghue, D., Beck, M., Harte, A., & Stott, D. (2006). Beneath the sand—remote sensing, archaeology, aggregates and sustainability: A case study from Heslerton, the Vale of Pickering, North Yorkshire, UK. *Archaeological Prospection*, *13*(4), 291–299. https://doi.org/10.1002/arp.297

Rowlands, A., & Sarris, A. (2007). Detection of exposed and subsurface archaeological remains using multi-sensor remote sensing. *Journal of Archaeological Science*, *34*(5), 795–803. https://doi.org/10.1016/j.jas.2006.06.018

Traviglia, A. (2006). MIVIS hyperspectral sensors for the detection and GIS supported interpretation of subsoil archaeological sites. In J. T. Clark, & E. M. Hagemeister (Eds.), *Digital discovery. Exploring new frontiers in human heritage. CAA2006. Computer applications and quantitative methods in archaeology. Proceedings of the 34th Conference, Fargo, United States, April 2006* (pp. 287–299). Archaeolingua: Budapest, Hungary.

Traviglia, A., Cowley, D., & Lambers, K. (2016). Finding common ground: Human and computer vision in archaeological prospection. *AARGnews – The Newsletter of the Aerial Archaeology Research Group*. 53, 11–24.

Verhoeven, G. (2009). Beyond conventional boundaries: New technologies, methodologies, and procedures for the benefit of aerial archaeological data acquisition and analysis. Ghent University, Belgium (PhD thesis).

Verhoeven, G., & Doneus, M. (2011). Balancing on the borderline – a low-cost approach to visualize the red-edge shift for the benefit of aerial archaeology: Balancing on the red-edge borderline. *Archaeological Prospection*, *18*(4), 267–278. https://doi.org/10.1002/arp.420

Verhoeven, G., & Sevara, C. (2016). Trying to break new ground in aerial archaeology. *Remote Sensing*, *8*(11), 918. https://doi.org/10.3390/rs8110918

Verhoeven, G., & Vermeulen, F. (2016). Engaging with the canopy—Multi-dimensional vegetation mark visualisation using archived aerial images. *Remote Sensing*, *8*(9), 752. https://doi.org/10.3390/rs8090752

Wilson, D. R. (2000). *Air photo interpretation for archaeologists*. Stroud, UK: Tempus.

How to cite this article: Moriarty C, Cowley DC, Wade T, Nichol CJ. Deploying multispectral remote sensing for multi-temporal analysis of archaeological crop stress at Ravenshall, Fife, Scotland. *Archaeological Prospection*. 2018;1–14. https://doi.org/10.1002/arp.1721